Lithos 388–389 (2021) 106076

Contents lists available at ScienceDirect

Lithos

journal homepage: www.elsevier.com/locate/lithos

Research Article

# Nature of the pre-collisional lithospheric mantle in Central Tibet: Insights to Tibetan Plateau uplift

Lin Ma [a,b,c,*], Qiang Wang [a,b,d], Andrew C. Kerr [c], Gong-Jian Tang [a,b]

[a] State Key Laboratory of Isotope Geochemistry, Guangzhou Institute of Geochemistry, Chinese Academy of Sciences, Guangzhou 510640, China
[b] CAS Center for Excellence in Deep Earth Science, Guangzhou 510640, China
[c] School of Earth and Environmental Sciences, Cardiff University, Cardiff, Wales CF10 3AT, United Kingdom
[d] University of Chinese Academy of Sciences, Beijing 100049, China

ARTICLE INFO

*Article history:*
Received 17 January 2021
Received in revised form 24 February 2021
Accepted 26 February 2021
Available online 4 March 2021

*Keywords:*
Late Mesozoic
Oceanic island basalt
Carbonated lithospheric mantle
Inherited mantle
Tibetan Plateau

ABSTRACT

The properties of accreted terranes in a large collisional orogen determine, in large part, the nature and subsequent development of the orogen. In this paper we present a detailed study of Late Mesozoic sodic mafic magmatic rocks from Central Tibet. These sodic mafic rocks from Bandatso provide an excellent opportunity to assess the nature and evolution of pre-collisional lithospheric mantle in the Himalayan–Tibetan region, and will thus aid our understanding of the evolution of the orogeny. The Bandatso sodic mafic rocks are characterised by marked oceanic island basalt (OIB)-like enrichment in incompatible elements, such as Nb (up to 139 ppm) and light rare-earth elements. This Late Mesozoic (ca. 148 Ma and 90 Ma) mafic magmatism is likely to be the result of two-stage mantle evolution in the northern Qiangtang. The late Jurassic rocks were derived from carbonated lithosphere metasomatized by subducted oceanic sediments during flat subduction. Whereas the late Cretaceous basanites were likely derived from interaction of lithosphere with upwelling asthenosphere induced by removal of lithosphere that had previously been thickened by relamination. Our study suggests the presence of an inherited carbonated lithospheric mantle beneath the northern Qiangtang prior to continental collision. The conclusions from this work suggest that the enrichment of the mantle source of Cenozoic potassic rock closely related to plateau uplift, more likely result from continental subduction after the late Cretaceous (ca. 90 Ma). These conclusions will help our understanding of the Cenozoic geology of this multi-terrane collision system and uplift mechanism of the Tibetan Plateau.



## 1. Introduction

The Himalayan-Tibetan orogen was formed by the accretion of a series of Gondwana-derived terranes and subsequent collision of the Indian and Asian continents (e.g., Chung et al., 2005; Murphy et al., 1997; Yin and Harrison, 2000; Zhu et al., 2013). Formation of the Tibetan Plateau has not only significantly affected the landscape of the Earth and the Cenozoic climate system (Dupont-Nivet et al., 2007; Royden et al., 2008), but also resulted in many significant geological processes (e.g., Chung et al., 2005; Kapp and DeCelles, 2019; Kelly et al., 2020). These include large-scale crust shortening (Kapp and DeCelles, 2019; Zhang et al., 2004), markedly different lithospheric composition and structure between the southern and northern plateaus (Chung et al., 2005; Deng and Tesauro, 2016), potential removal of lithosphere (e.g., Chen et al., 2017; Shi et al., 2020) and continuous migration of Cenozoic magmatism between the Qiangtang and Lhasa terranes (Chung et al., 2005; Kapp and DeCelles, 2019).

Various models have been proposed to explain uplift of the Tibetan Plateau. Delamination of the overthickened lithosphere (Chen et al., 2017; Chung et al., 1998; England and Houseman, 1986; Shi et al., 2020; Turner et al., 1993, 1996) and continental subduction (Ding et al., 2003; Guo et al., 2015; Guo and Wilson, 2019; Harrison et al., 1992; Ma et al., 2017; Tapponnier et al., 2001) are two of particular significance. Both models have been presented as an explanation for formation of the Cenozoic potassic rocks in Tibet (e.g., Chung et al., 1998; Ding et al., 2003; Guo et al., 2006, 2015; Ma et al., 2017; Turner et al., 1993, 1996). The focus of the debate concerns the role of continental subduction in formation of an enriched mantle source of the Cenozoic potassic rocks. The first model attributes such enriched mantle to inherited subcontinental lithospheric mantle (SCLM) during oceanic slab subduction, whereas the second model emphasizes the role of continental subduction. Goussin et al. (2020) have proposed the presence of a carbonated lithospheric mantle below the eastern Qiangtang based on the mantle phlogopite xenocrysts preserved in Eocene potassic rocks. Although when and how such a lithospheric mantle formed

* Corresponding author at: State Key Laboratory of Isotope Geochemistry, Guangzhou Institute of Geochemistry, Chinese Academy of Sciences, Guangzhou 510640, China.
*E-mail address:* malin@gig.ac.cn (L. Ma).

https://doi.org/10.1016/j.lithos.2021.106076
0024-4937/

may be crucial in helping to revolve conflicting interpretations of the geophysical data, little is known about this carbonated mantle. Numerical geodynamical modelling experiments also show that the inherited properties of the mantle lithosphere of the accreted Asian upper-plate are key to unravelling the enigmatic post-collisional behaviour of the Himalayan-Tibetan orogeny (Kelly et al., 2020).

Only a few reports of magmatic rocks constrain the properties and compositions of pre-collisional lithospheric mantle in the northern Qiangtang after closure of Paleo-Tethyan ocean in the Triassic (~233 Ma, Dan et al., 2020; Zhang et al., 2016) until the Cenozoic (Deng, 1998; Ding et al., 2003; Guo et al., 2006). Therefore, in this contribution, we present new geochronology, petrology and geochemical data for the Late Mesozoic sodic mafic magmatic rocks from the northern Qiangtang. These mafic rocks present a rare opportunity to constrain the nature and composition of the lithospheric mantle beneath the northern Qiangtang region prior to Indo-Asian collision and provide insights into the post-collisional evolution of Himalaya-Tibet orogen and uplift mechanism of Tibetan Plateau.

## 2. Geological background and sampling

The Tibetan Plateau consists of a tectonic collage of crustal blocks. From north to south, the main east–west-trending blocks are the Kunlun–Qaidam, Songpan-Ganze, Qiangtang, Lhasa and Himalaya Blocks (Fig. 1) (Chung et al., 2005; Yin and Harrison, 2000). These blocks are separated by a series of suture zones, namely the Anyimaqen–Kunlun–Muztagh, Jinsha, Bangong-Nujiang, and Indus-Yarlung Tsampo Suture Zones (Fig. 1).

The Qiangtang Block, located in central Tibet, can be divided into southern and northern sub-blocks separated by an early Mesozoic blueschist-bearing metamorphic belt named the Longmutso-Shuanghu Suture (LSS) zone (Fig. 1; e.g., Zhang et al., 2016 and references therein). Although there is still controversy as to which of the Jinsha and Longmutso-Shuanghu suture zones represents the final closure location of the Paleo-Tethys Ocean basin (e.g., Zhang et al., 2016; Zhu et al., 2013 and references therein), both models suggest that the Paleo-Tethys Ocean closed in the Early Triassic (prior to 220 Ma, Dan et al., 2020; Xu et al., 2020; Zhang et al., 2016). Following this closure, magmatism in the Northern Qiangtang terrane was rare until the Cenozoic (e.g., Xu et al., 2020; Zhu et al., 2013). Before the magmatic gap at 150–130 Ma, Jurassic magmatism and metamorphism were mainly focussed within the Bangong-Nujiang suture zone and are only rarely found in Qiangtang (Liu et al., 2016; Peng et al., 2020; Tang et al., 2020; Zhang et al., 2017) and references therein). This is likley related to the angle of subduction (normal or steep) of the Bangong-Nujiang Tethyan slab during early Jurassic (prior to 170 Ma). Cenozoic igneous rocks are sporadically distributed in the Qiangtang terrane but are mainly clustered in the northern part of the block close to the Jinsha suture (Fig. 1). Early Paleogene (ca. 60–45 Ma) Na-rich alkali basalts occur in the northwest Qiangtang terrane (e.g., Deng, 1998; Ding et al., 2003), while Eocene–early Oligocene (ca. 50–28 Ma) potassic volcanic and subordinate intrusive rocks are widely distributed throughout the Qiangtang terrane (Fig. 1) (e.g., Chung et al., 2005; Ding et al., 2003, 2007; Guo et al., 2006; Ou et al., 2017, 2019; Wang et al., 2008, 2010).

The Na-rich basalts are characterised by high $Mg^{\#}$ and Cr, Ni contents and have been proposed to represent primitive mantle melts during roll-back of a previously shallow subducted Neo-Tethyan slab (e.g., Deng, 1998; Ding et al., 2003). Subsequent potassic magmas were derived from an enriched mantle source during continental subduction (e.g., Ding et al., 2003; Guo et al., 2006) or lithospheric delamination (e.g., Chung et al., 2005; Turner et al., 1993).

The study area is located in the hinterland of the plateau about 150 km northeast of Songxi town (Fig. 1) at an altitude of 5500 m. The studied sodic mafic rocks, including basanite and dolerite, occur as volcanic hills and dykes (Fig. 2 and S1a–d) and are mainly distributed on the north and south sides of Bandatso Lake over an area of about ~200 $km^2$. These mafic rocks were erupted on to, or were emplaced into, the Paleozoic neritic facies deposits and their distribution appears to be controlled by SW-NE trending faults (Fig. 2).

The Bandatso basanites consists of subhedral and anhedral plagioclase and clinopyroxene phenocrysts, and secondary carbonate, set in a fine grained and glassy groundmass (Fig. 3e, f). The Bandatso dolerites are composed of clinopyroxene (40–60%), plagioclase (30–50%), and Fe—Ti oxide, apatite (Fig. 3g, h). Some clinopyroxenes have a needle-like texture (Fig. 3g, h). The minerals are randomly oriented, indicating that they formed in flowing magma rather than accumulation of crystals (Fig. 3g, h).

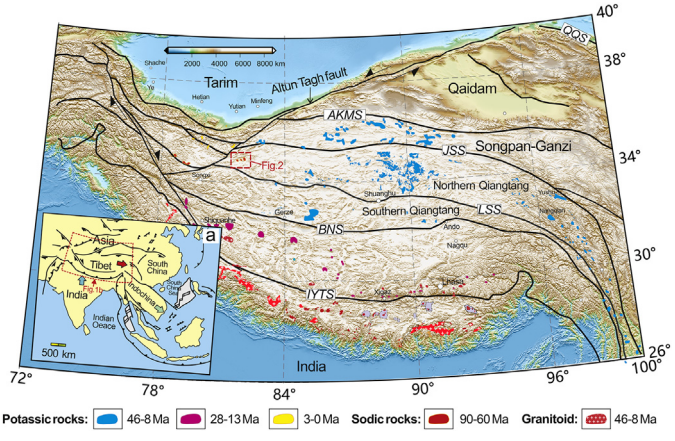


**Fig. 1.** A topographic map of Tibet showing the tectonic blocks and the location of Cenozoic magmatic rocks in Tibetan Plateau. Abbreviations: Indus-Yarlung Tsampo suture (IYTS); Bangong-Nujiang suture (BNS); Longmutso-Shuanghu suture (LSS); Jin-Sha suture (JSS) and Anymaqen-Kunlun-Muztagh Suture (AKMS). The Cenozoic magmatic rock data is from literatures (Chung et al., 2005; Ding et al., 2003; Ma et al., 2019; Ou et al., 2019). The original digital topography data for the Tibetan Plateau are from the Earth Resources Observation and Science (EROS) Center of United States Geological Survey (http://eros.usgs.gov/products/elevation/gtopo30.html).

## 3. Analytical methods

Argon isotope analyses of plagioclase from three samples were conducted on a multi-collector ARGUS VI Noble Gas Mass Spectrometer at the Laboratory in China University of Geosciences (Wuhan) following procedures similar to those described in detail by Bai et al. (2018). All samples were stepwise heated using a carbon dioxide infrared laser (10.6 μm, 50 W). The $^{40}Ar—^{39}Ar$ dating results were calculated and plotted using the software ArArCALC (Version 2.52) (Koppers, 2002). The $^{40}Ar—^{39}Ar$ age data are listed in Table S1.

Rock samples were first examined by optical microscopy and the freshest whole-rock samples were broken into small chips. These chips were washed with distilled water before being dried and handpicked to remove visible contamination. The rocks were powdered before analysis of major and trace elements, and Sr—Nd isotopes at SKLaBIG GIG CAS. Major-element oxides were determined by a Rigaku RIX 2000 X-ray fluorescence spectrometer on fused glass beads with analytical uncertainties <5%. Trace elements were analysed by a Perkin–Elmer Sciex ELAN 6000 instrument. Trace element data of reference materials (DM17-1, AD01-1, AD02-2, AD02-8, SARM-4, W-2a, BHVO-2, GSR-2, AGV-2, GSR-3, GSR-1) are given in Table S4.

Sr and Nd isotopic compositions of selected samples were determined using a MC-ICP-MS at SKLaBIG, GIG–CAS. The $^{87}Sr/^{86}Sr$ ratio of the NBS987 standard and $^{143}Nd/^{144}Nd$ ratio of the Shin Etsu JNdi–1 standard measured were 0.710260 ± 6 (2σ, $n = 17$) and 0.512103 ± 5 (2σ, $n = 19$), respectively. All measured $^{143}Nd/^{144}Nd$ and $^{86}Sr/^{88}Sr$ ratios are fractionation corrected to $^{146}Nd/^{144}Nd = 0.7219$ and $^{86}Sr/^{88}Sr = 0.1194$, respectively.

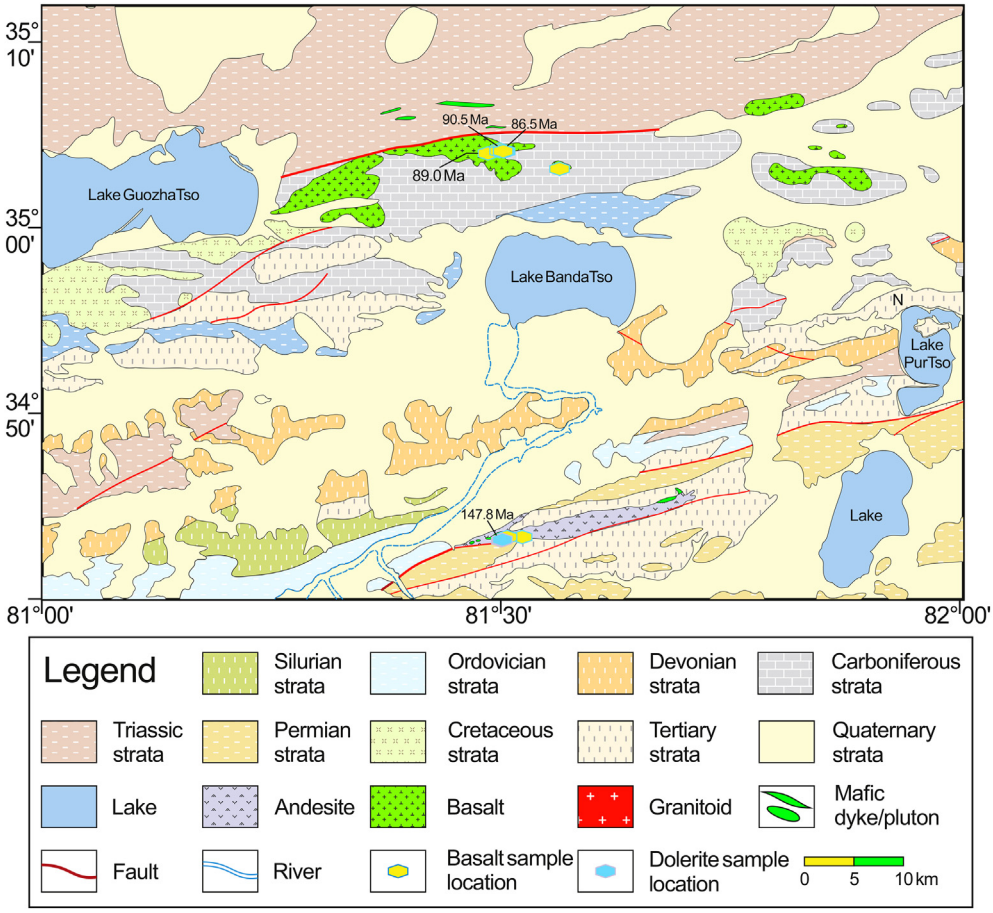


**Fig. 2.** Geological map showing the location of the sodic mafic rocks in this study.

## 4. Results

### 4.1. Plagioclase $^{40}Ar$—$^{39}Ar$ dating

Plagioclases from one dolerite sample (14QW67) and three basaltic samples (14QW18, 14QW22 and 14QW55) were selected for $^{40}Ar$—$^{39}Ar$ dating. The plagioclase from dolerite sample 14QW67 gave a late Jurassic plateau age of 147.8 ± 1.2 Ma, which is the first report on the age of late Jurassic mafic rocks in northern Qiangtang. The plagioclase of Bandatso basanite samples (14QW18, 14QW22 and 14QW55) in this study yielded $^{40}Ar$—$^{39}Ar$ plateau ages of 90.5 ± 1.0 Ma, 86.5 ± 7.1 Ma and 89.0 ± 3.6 Ma, respectively (Fig. 4; Table S1). The Bandatso basalts were previously thought to have formed in the Eocene coeval with other Na-rich mafic rocks in the northern Qiangtang based on unpublished $^{40}K$—$^{40}Ar$ data (e.g., Chung et al., 2005; Ding et al., 2003). Our new geochronological data of Bandatso basalts indicates that this is incorrect and that the Bandatso basaltic lavas were formed in the Late Cretaceous (91–87 Ma, weighted mean age: 90.32 ± 0.95 Ma) (Fig. 4).

### 4.2. Major and trace elements

The major and trace element data for 29 samples are given in Table S2. The samples classify as either alkaline basalt or basanite compositions (Fig. 5), with sodium/potassium ratios up to 16.4 (with mean of 3.6). All these Late Mesozoic sodic rocks are characterised by low $SiO_2$ and $K_2O$ contents and they are markedly different from the Eocene-Miocene potassic to ultra-potassic magmatic rocks in Qiangtang and Songpan-Ganze region (Fig. 5).

The rocks in this study show a wide range in $SiO_2$ (38.8–50.1 wt%) and MgO (3.6–9.4 wt%) with relatively high $TiO_2$ (1.5–3.7 wt%) contents (Table S2). Four samples (14QW58, 14QW60, 14QW62 and 14QW63) have high loss on ignition (L.O·$I$ > 6 wt%) and so in the following discussion we will only use the immobile element data for these samples, to avoid the potential effects of element mobility due to alteration.

The Bandatso mafic rocks are characterised by variable and enriched light rare earth elements (LREEs) ($[La/Sm]_N$ = 1.4–8.7) and depleted heavy REE ($[Dy/Yb]_N$ = 1.5–2.3) with insignificant Eu anomalies ($Eu/Eu^* = Eu/\sqrt[2]{Sm \times Gd}$ = 0.92–1.01) (Fig. 6a). Primitive mantle-normalised trace-element patterns show significant enrichments in high field strength element signatures (HFSE; e.g., Nb, Ta) and variable large ion lithophile elements (LILEs; e.g., Sr and Ba) with negative Th—U anomalies ($[Th/La]_{PM}$ = 0.31–0.97) (Fig. 6). These features are distinct from those of continental crust and arc-like basalts that are characterised by LILE-rich and HFSE-poor signatures (e.g., Rudnick and Gao, 2003; Tatsumi and Eggins, 1995).

Nevertheless, the late Cretaceous Bandatso basanite and late Jurassic dolerite samples exhibit distinct differences in their geochemical compositions, such as REE and HFSE contents (Fig. 6b, Table S2). Late Cretaceous basanites have high total REE (187–320 ppm) and Nb (51–87 ppm) contents and positive Nb—Ta anomalies ($[Nb/La]_{PM}$ = 1.08–1.43; $Nb/Nb^* = 2 \times Nb_N/(Th_N + La_N)$ = 1.19–1.45) (Fig. 6), whereas Late Jurassic dolerites have higher total REE (800–1022 ppm) and Nb (73–139 ppm) contents with moderate negative Nb ($Nb/Nb^*$ = 0.41–0.60) and Zr-Hf-Ti anomalies (Fig. 6).

### 4.3. Sr—Nd isotopes

Sr and Nd isotope results for 8 representative Bandatso samples are shown in Table S3. The late Cretaceous samples have positive $\varepsilon_{Nd}$ (t) (+0.03 − +2.37) values and relatively low $(^{87}Sr/^{86}Sr)_i$

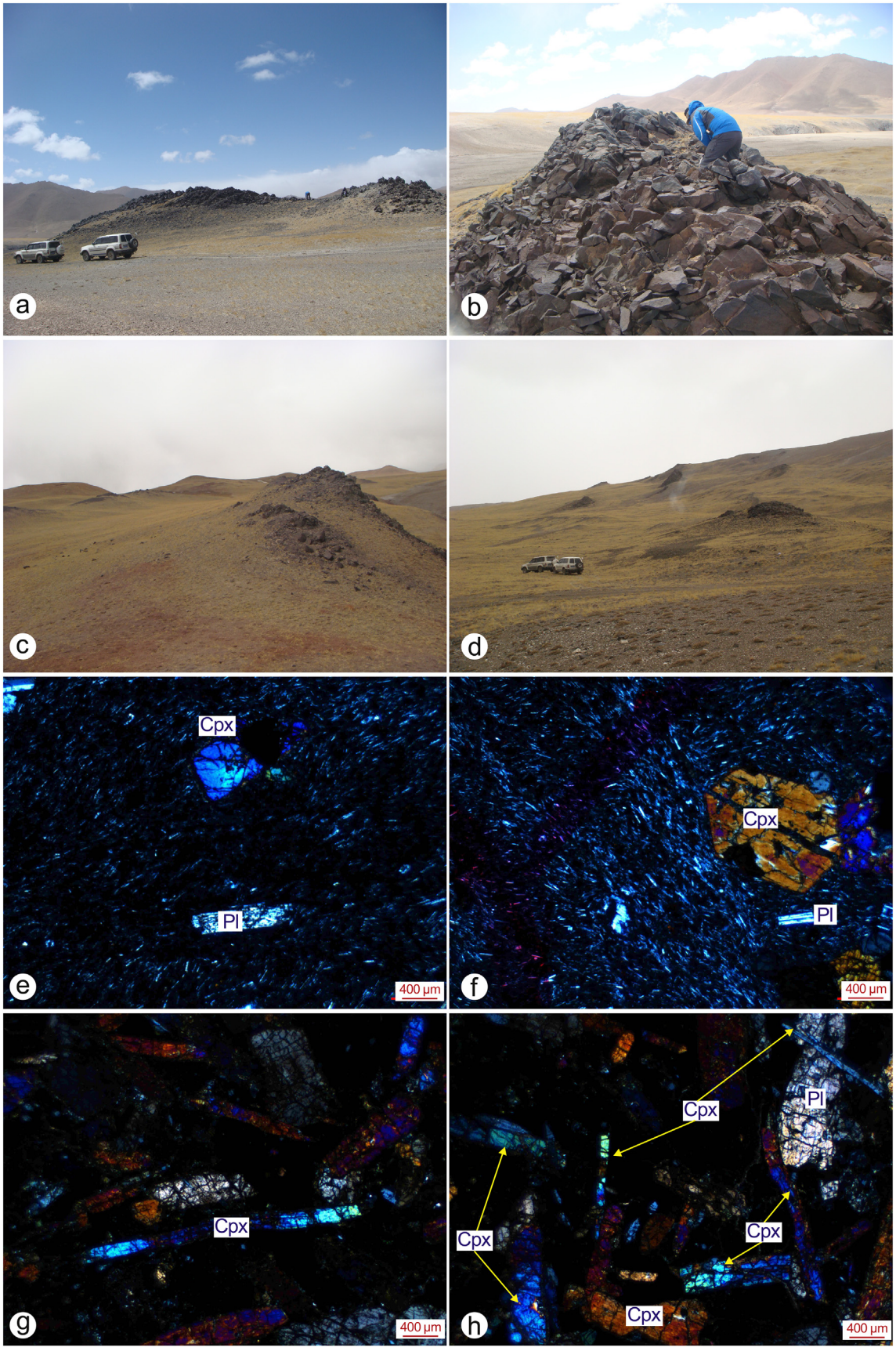


**Fig. 3.** field and petrography pictures. (a-d) The field outcrop of the Bandatso mafic rocks; (e-f) Micro-petrographic photos of the Bandatso basanite; (g-h) Micro-petrographic photos of the Bandatso dolerite.

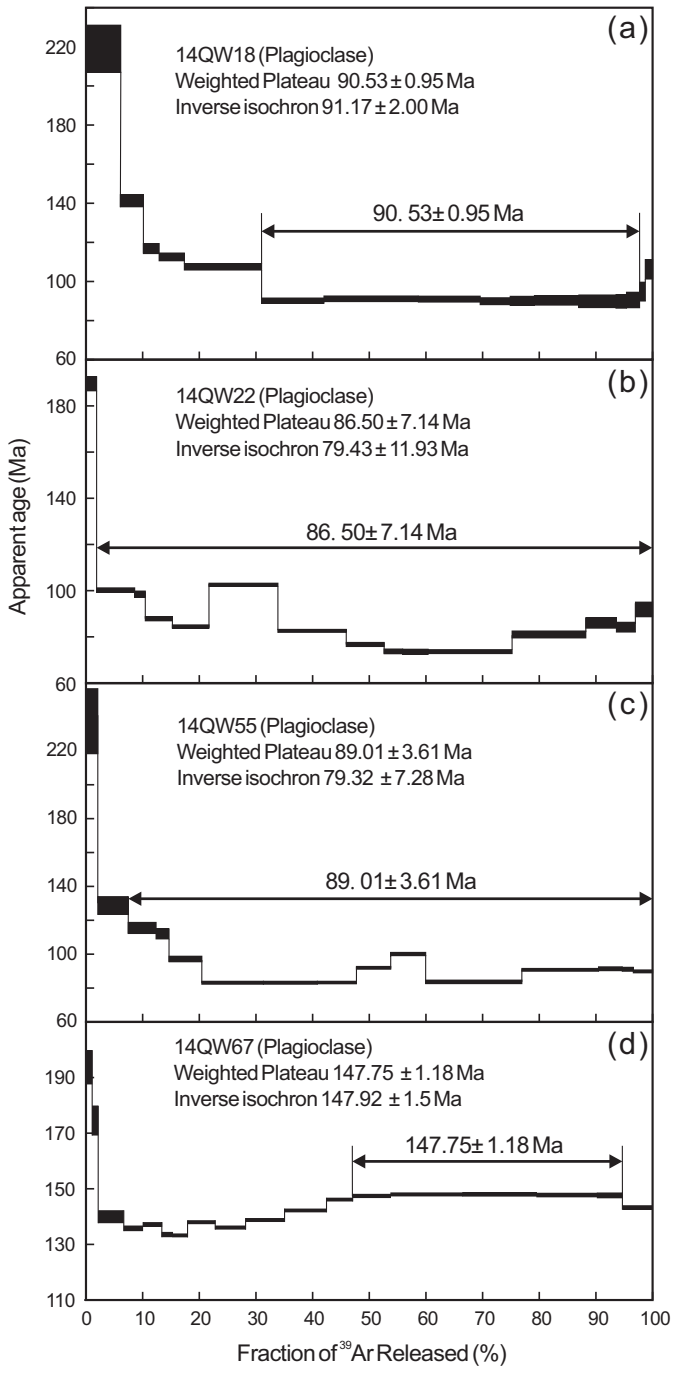


**Fig. 4.** Incremental-heating spectra of $^{39}Ar/^{40}Ar$ for plagioclase from three Bandatso sodic mafic rocks. (a) the sample 14QW18 yield reproducible plateaus (90.5 ± 1.0 Ma); (b) the sample 14QW22 yields a plateau (86.5 ± 7.1 Ma); (c) the sample 14QW55 yield the plateaus (89.0 ± 3.6); (d) the sample 14QW67 yield the plateaus (147.8 ± 1.2).

(0.7043–0.7049) (Fig. 7), whereas the late Jurassic samples have negative $\varepsilon_{Nd}(t)$ (−0.64 to −0.36) values and much higher $(^{87}Sr/^{86}Sr)_i$ (0.7041–0.7046) ratios (Fig. 7).

## 5. Discussion

### 5.1. Fractional crystallisation and crustal assimilation

Fractional crystallisation with concurrent crustal assimilation can mask primary magma compositions, and thus may hamper a straightforward interpretation of trace element data with respect to the nature

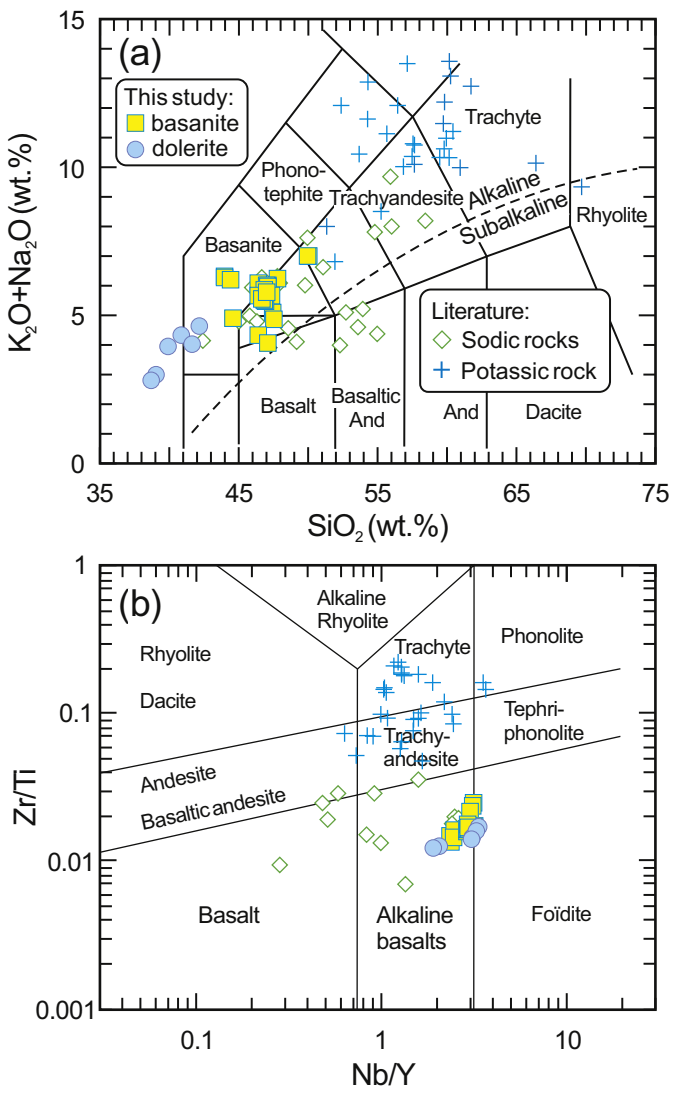


**Fig. 5.** (a) $SiO_2$ versus $K_2O + Na_2O$ plot (Le Bas et al., 1986) and (b) $Zr/TiO_2 \times 0.0001$ versus Nb/Y plot (Pearce and Peate, 1995). Data for Cenozoic alkaline mafic rocks of the Qiangtang are provided for comparison and are from Deng (1998) and Ding et al. (2003). The Lagala, Bandatso, Hongshanhu and Tongtianqiao samples are sodic rocks, whereas the Yulingshan and Chazi-Wenbu samples are potassic rocks.

and composition of the melt source region (e.g., Hastie et al., 2011). Evaluation of these magma chamber processes is thus required before conclusions on the origin and source of basaltic magmas can be drawn from element and isotope data.

#### 5.1.1. Fractional crystallisation

Linear trends on variation diagrams of major and trace elements for the two suites of Bandatso mafic rocks indicate the likelihood of fractional crystallisation (Hastie et al., 2011). In the following section we will assess the potential influence of olivine, pyroxene and plagioclase fractionation on the composition of the Bandatso mafic rocks.

Insignificant Eu anomalies ($Eu/Eu^* = 0.92–1.01$) indicate a limited amount of plagioclase crystallisation in the Bandatso mafic rocks. Increasing $Al_2O_3$ contents with magmatic evolution (i.e., MgO reduction) also does not support the significant fractionation of plagioclase. Similarly, the lack of correlation between CaO and MgO suggest that the late Cretaceous Bandatso basanites did not undergo much fractional crystallisation of clinopyroxene (Fig. S1). In contrast, the positive correlation of CaO and $Fe_2O_3$ with MgO indicate that the late Jurassic samples likely underwent significant fractional crystallisation of clinopyroxene

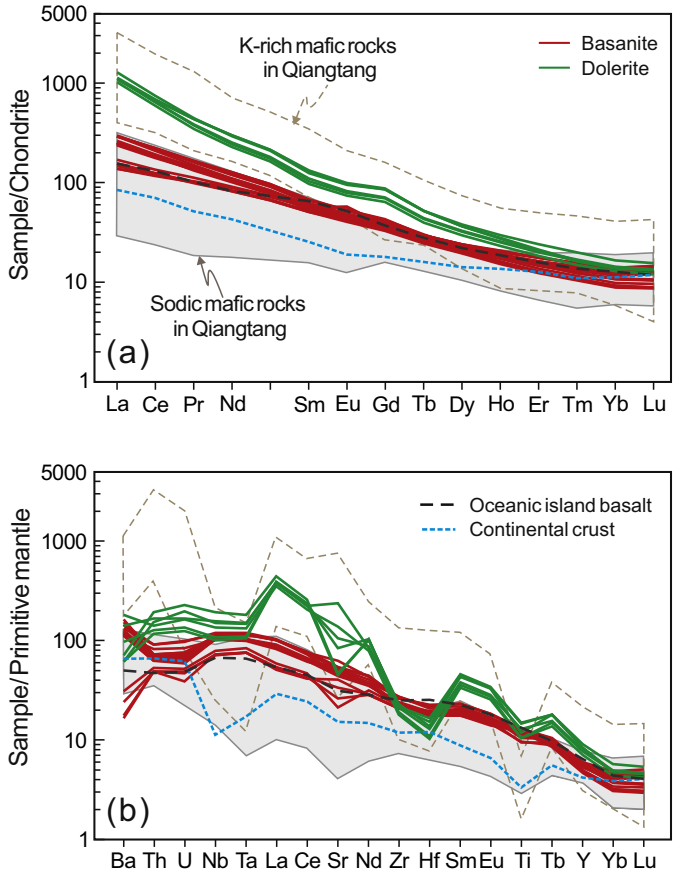


**Fig. 6.** (a) Chondrite-normalised REE and (B) primitive mantle-normalised multi-element patterns for the Yegai potassic rocks. The data of Cenozoic K-rich and sodic mafic rocks in Qiangtang are from Ding et al. (2003) and Deng (1998). The chondrite and primitive mantle normalization values are from Sun and McDonough (1989).

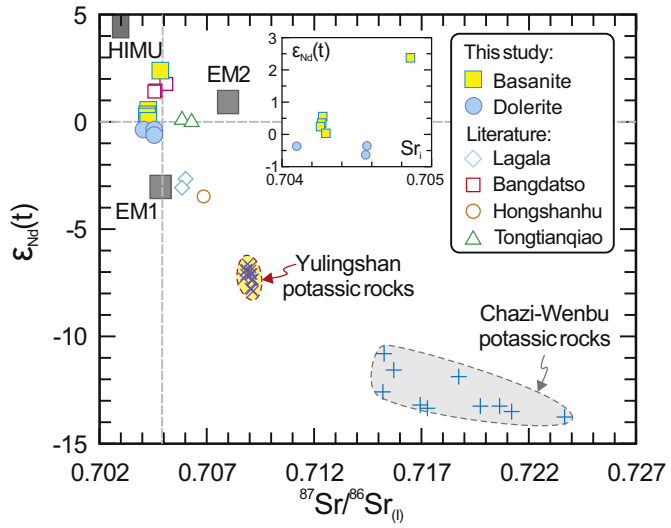


**Fig. 7.** $\varepsilon_{Nd}(t)$ vs $(^{87}Sr/^{86}Sr)_i$ diagram. Data for Cenozoic alkaline mafic rock of the Qiangtang are provided for comparison and are from Deng (1998) and Ding et al. (2003). The data of OIB endmembers (EM1, EM2 and HIMU) are from Hart et al. (1992) and Jackson and Dasgupta (2008).

(Fig. S1). The significant decrease in Cr and Ni contents with falling MgO does however indicate that olivine was a major crystallising phase from all of the Bandatso mafic rocks (Fig. S1h, i). It is also important to note that Nb contents appear to indicate minimal fractional crystallisation of rutile or Fe—Ti oxides, based on weak to moderate negative correlation of Nb with MgO and $TiO_2$ (Fig. S1g, k).

In conclusion, olivine fractional crystallisation is most likely responsible for the variation of major and trace elements in the Bandatso mafic rocks. In addition to this the late Jurassic samples probably underwent minor fractional crystallisation of clinopyroxene.

*5.1.2. Crustal contamination*

Continental crust is characterised by enrichment in LILE and depletion in HFSE, such as Nb and Ta (e.g., Rudnick and Gao, 2003). However, all Bandatso basaltic samples show significantly higher Nb contents and Nb/U ratios than continental crust (Fig. 8a; Hofmann, 1997). If there is crustal contamination, it will have had little influence on the trace element and isotopic signature, given that these rocks are so enriched. Moreover, the lack of an increase in $(^{87}Sr/^{86}Sr)_i$ and decrease in $(^{143}Nd/^{144}Nd)_i$ with increasing $SiO_2$ and decreasing MgO and Nb/La, likewise does not support significant crustal contamination (Fig. 9). Therefore, combined with low $SiO_2$ and high MgO contents of the Bandatso basaltic samples, there is very little evidence that crustal contamination has a significant effect on the composition of these rocks.

*5.2. Magma source region*

Enriched incompatible elements and high Nb contents of the Late Mesozoic Bandatso rocks are markedly different from mid-ocean ridge basalt (MORB) and subduction-related basalts (Fig. 6). In addition, there is little evidence for hotspot-related magmatism in the study region during late Triassic to the present-day. Thus, there is unlikely to have been a plume beneath the Central Tibet during the Late Mesozoic.

Instead, we propose that the late Jurassic Bandatso dolerites were derived from a carbonatite metasomatised lithospheric mantle. Carbonatite contamination of a peridotite source region would produce high and fractionated Zr/Hf ratios of up to 100 in any resultant melt (Chauvel et al., 1997; Woodhead, 1996), which is in contrast to the average Zr/Hf ratios (~33–49) for MORB, continental flood basalts, arc basalts and some OIB lavas (Chazot et al., 1996; Dupuy et al., 1992; Woodhead, 1996). In addition, carbonatite melts and the contaminated sources, have very high LREEs concentrations (> > 100 times chondrite) and negative Ti anomalies on chondrite/primitive mantle-normalised multi-element diagrams (Chauvel et al., 1997; Hauri et al., 1993; Woodhead, 1996).

The late Jurassic Bandatso dolerite samples have high LREEs ($La_N$ = 1027–1313) and Nb (73–139 ppm) contents as well as somewhat elevated Zr/Hf (48–64) ratios with markedly negative Ti anomalies ($Ti/Ti^* = 2 \times Ti_N/(Sm_N + Tb_N)$ = 0.38–0.49) (Fig. 6, Table S2). These elevated Zr/Hf ratios probably reflect mantle source variably metasomatized by finite carbonate-rich fluids (Dupuy et al., 1992). Depletion in Ti, Zr, and Nb (as well as Sr) relative to the REE are similar to those found in continental xenoliths that have been metasomatized by a carbonaceous melt (Hauri et al., 1993; Zhang et al., 2017) and references therein), suggesting involvement of a carbonate-rich melt component. All these thus support the late Jurassic dolerite was derived from a carbonated lithosphere mantle source. In addition, the markedly distinct compositions of Bandatso dolerite from that of continental crust (Fig. 8), exclude the potential of significant continental crust component as the main metasomatic agent for mantle source during late Jurassic. The carbonate-rich fluid and melt components thus are more likely derived from recycled oceanic slab materials. The mantle phlogopite xenocrysts and carbonate-bearing ultramafic cumulates preserved in Eocene potassic rocks from the Eastern Qiangtang terrane also support such a pre-collisional carbonated lithospheric mantle beneath Central Tibet (Goussin et al., 2020).

The late Cretaceous Bandatso basanites are characterised by OIB-like compositions with positive Nb—Ta anomalies (Fig. 6b) and high Nb/U ratios (up to 63) comparable to MORB (49.6) and OIB (47.1) (Fig. 8). However, their low Th and U ($[Th/La]_{PM}$ = 0.31–0.97) compositions

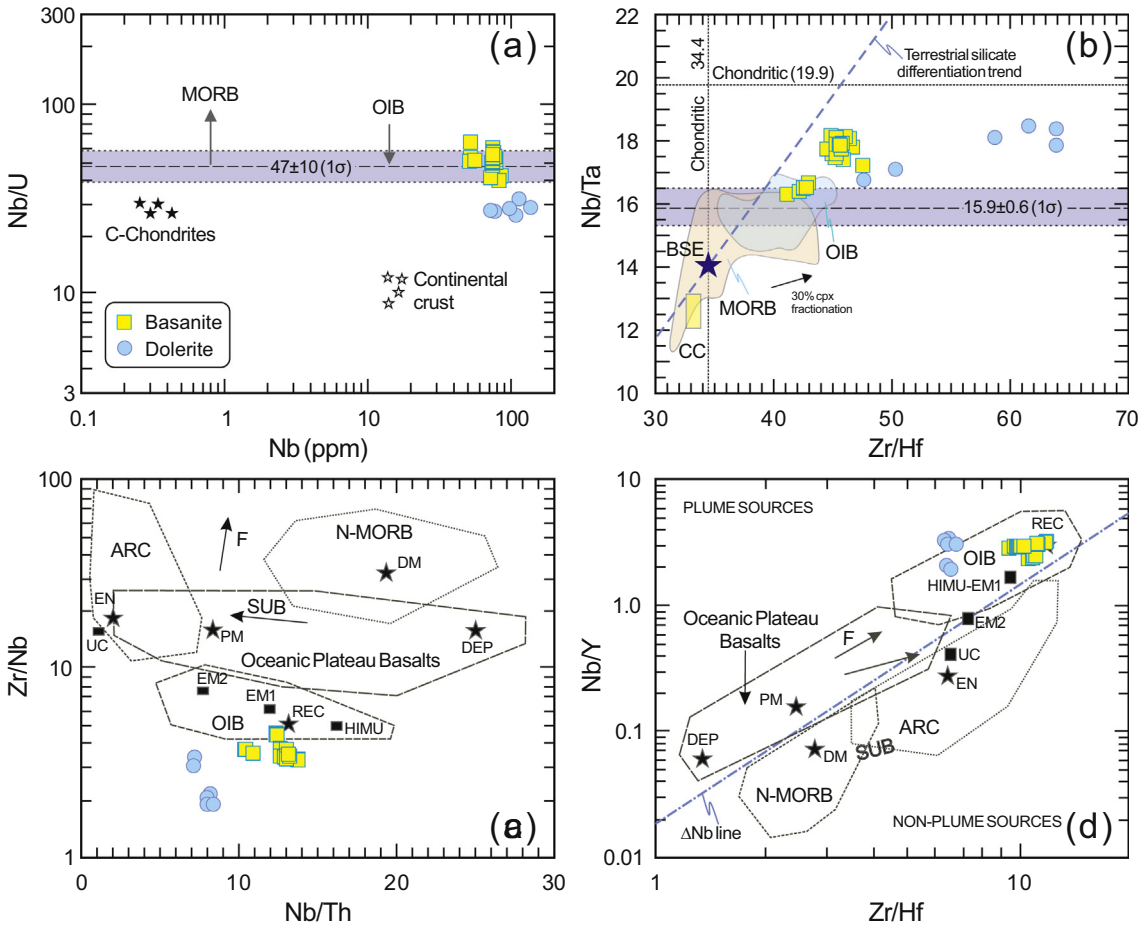


**Fig. 8.** Plots of Nb/U versus Nb (a), Nb/Ta versus Zr/Hf (b), Zr/Nb versus Nb/Th (c) and Nb/Y versus Zr/Hf (d). Data sources: (a) MORB, OIB, Continental crust and carbonaceous (C)-chondrite data are after Hofmann (1997); The purple field indicate the average OIB after Sun and McDonough (1989) and Pfänder et al. (2012). (b) MORB, OIB, Bulk Solid Earth (BSE), Continental Crust (CC) and chondrite data are after Pfänder et al. (2012) and references therein; (c, d) The fields of OIB, N-MORB, ARC and Oceanic Plateau Basalts endmembers data are from Condie (2005). ΔNb line distinguishing Plume and non-Plume series is from Condie (2005). Abbreviations: UC, upper continental crust; PM, primitive mantle; DM, shallow depleted mantle; HIMU, high mu (U/Pb) source; EM1 and EM2, enriched mantle sources; ARC, arc related basalts; N-MORB, normal ocean ridge basalt; OIB, oceanic island basalt; DEP, deep depleted mantle; EN, enriched component; REC, recycled component. F indicates the trend for higher melting degree than 10–20% of tholeiite. SUB indicates addition of more subduction materials.

are inconsistent with a source containing recycled oceanic sediments e.g., HIMU (high-μ, $\mu = {}^{238}U/{}^{204}Pb$). Moreover, the average Th/Nb ratio of the late Cretaceous samples is 0.072 whereas the ratios for enriched mantle (EM)-1, EM-2 type OIB are 0.10–0.12 and 0.11–0.16, respectively (e.g., Woodhead, 1996). The depleted mantle-like Sr—Nd isotope signatures and marked enrichment of incompatible elements also do not support a source containing recycled continental crust and oceanic crust. Given the lack of evidence for coeval mantle plume in Qiangtang mentioned above, the late Cretaceous Bandatso sodic basanites thus are unlikely to be derived from an OIB-type mantle reservoir (e.g., EM1, EM2 or HIMU) (Hofmann, 1997). The relatively depleted Sr—Nd isotopic compositions (Fig. 7) and higher Nb and lower LREE contents than that of late Jurassic dolerite, suggests involvement of depleted asthenosphere in the generation of the late Cretaceous Bandatso basanites. It is therefore more likely that late Cretaceous sodic basanites were derived from interaction between asthenospheric melts and metasomatised lithosphere, and this possibility will be explored below.

### 5.3. Primitive magmas and properties

Mantle-derived alkaline lavas rich in alkali metals such as potassium and sodium are commonly found in the interiors of continental and oceanic plates (e.g., McKenzie and O'Nions, 1995; Hofmann, 1997; Niu, 2008; Lee et al., 2009). These small-volume alkaline magmas have variously been proposed to be derived from mantle plumes (Hofmann, 1997; Wang et al., 2015; Yang and Faccenda, 2020) or metasomatised lithospheric mantle (McKenzie and O'Nions, 1995; Pilet et al., 2008; Yang and Faccenda, 2020), and thus provide an excellent proxy with which to probe the compositional and physical properties of the deep mantle (e.g., Lee et al., 2009).

The thermal state of the mantle can be constrained by the temperatures and pressures of coeval basaltic magma generation(e.g., Herzberg et al., 2007; Lee et al., 2009; McKenzie and Bickle, 1988; Putirka, 2008). Accordingly, in this study, we have used six of the most primitive and least fractionated samples to calculate the primary melt composition and to assess the thermal state of the mantle beneath the Central Tibet during late Mesozoic (148 Ma to 90 Ma). To minimize the effect of olivine and clinopyroxene fractionation, only samples with MgO > 7.0 wt% were selected.

Olivine increments are required to be in equilibrium with the instantaneous melt composition, assuming compositionally dependent olivine/melt $KD_{(Fe/Mg)}$ of 0.3 (Tamura et al., 2000). Such olivines were back-added to melt until the $Mg^{\#}$ reached ranges between 71 and 81, when the magma composition is considered to be in equilibrium with a mantle composition (Albarede, 1992). This mantle composition is assumed to be the average composition of the mantle residue after melt

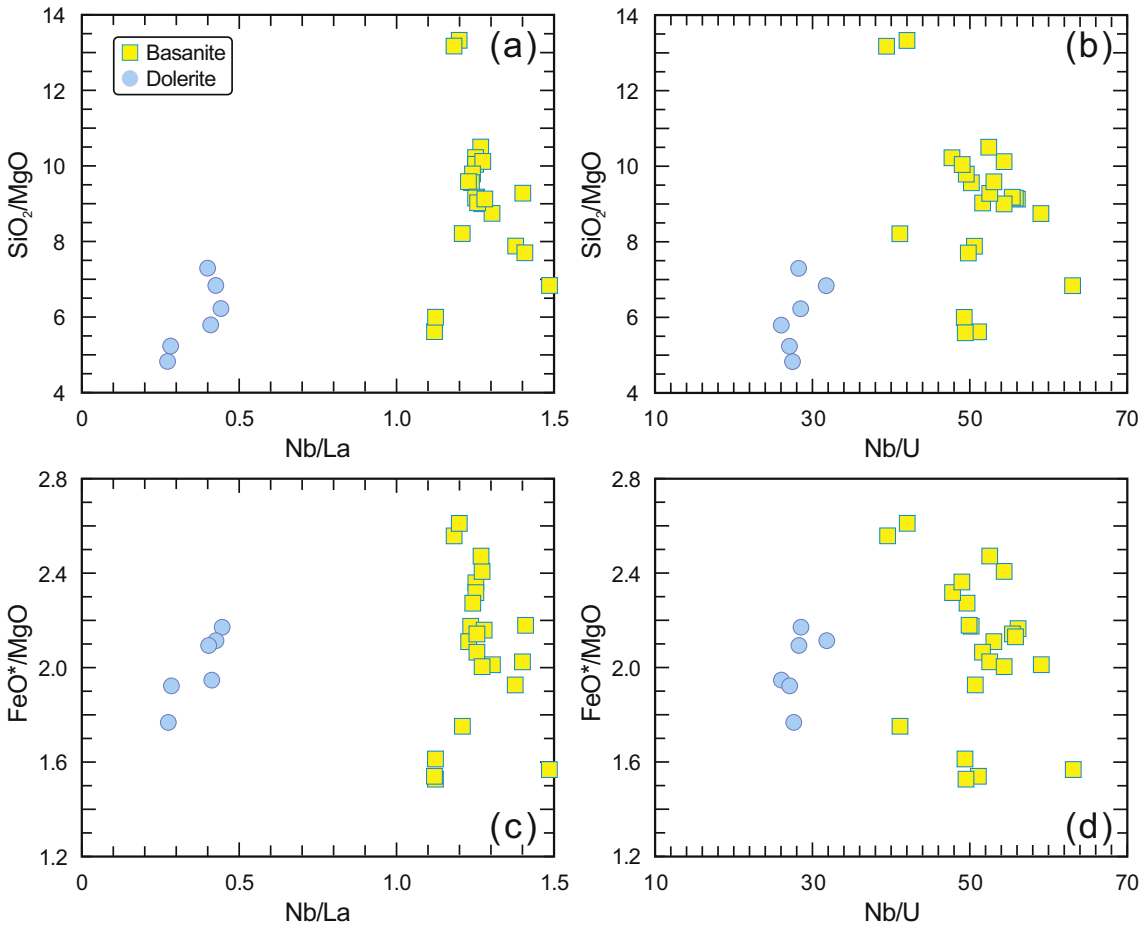


**Fig. 9.** Plots of $SiO_2$/MgO versus Nb/La (a) and Nb/U (b), FeO*/MgO versus Nb/La (c) and Nb/U (d).

extraction (Albarede, 1992). A series of olivine and basalt compositions were then calculated from these starting materials as follows: (1) the composition of equilibrium olivine was obtained using $KD_{(Fe/Mg)}^{oliv/liq} = 0.31$ (Putirka, 2005) and $D_{Ni}^{oliv/liq}$ (Beattie et al., 1991), assuming that $Fe^{2+}/(Fe^{2+}+Fe^{3+}) = 0.90$ in the melt (Lee et al., 2009); (2) a more primitive basalt composition was calculated as a mixture of the basalt and equilibrium olivine in a weight ratio of 99.9:0.1 (Wang et al., 2011); (3) steps 1 and 2 were repeated using the calculated primitive basalt to obtain a more primitive basalt.

Given the likely carbonatite contaminated peridotite source, the primary melts of late Jurassic dolerite were calculated until equilibrium with Fo87 olivine, similar to fertile mantle (after Sobolev et al., 2005). Other Bandatso samples were calculated assuming liquid $Mg^{\#}$ values consistent with a Fo89 source (Lee et al., 2009). The amounts of olivine addition are mostly between 21% and 24% for the Bandatso mafic rocks (Table S5).

An independent constraint on the primary melt compositions can be obtained by comparing the compositions calculated by another model of olivine addition (Herzberg and Asimow, 2008; Herzberg and O'hara, 2002). The major oxide contents calculated by the two different models are similar, suggesting that the calculated primary magmas represent primary melt compositions. The calculated primary melts of late Jurassic dolerites have low $SiO_2$ (39.5–41.2 wt%) and high MgO (14.4–14.7 wt%) contents, whereas the estimated primary magma compositions of late Cretaceous basanites are characterised by similar MgO (14.2–14.7 wt%) contents but slightly higher $SiO_2$ (43.7–46.5 wt%) (Table S5). $H_2O$ contents were calculated by assuming that the primary magma has $H_2O$/Ce ratio of ~200 similar to oceanic basalt (Herzberg et al., 2007).

Four separate thermometers were used to estimate the mantle potential temperature of the Bandatso basalts (Albarede, 1992; Herzberg et al., 2007; Lee et al., 2009; Sugawara, 2000). Given that the effect of water is not considered in some calculations, we subtracted the difference in temperature due to water as $\Delta T = 74.403 \times (H_2O\ wt\%)^{0.352}$ (Falloon and Danyushevsky, 2000).

The details of initial and calculated compositions and mantle potential temperature and pressure along with melting proportions, are shown in Table S5. The late Jurassic samples from the carbonatite contaminated fertile mantle have moderate mantle potential temperatures (1225–1240 °C), whereas all late Cretaceous basanites yield higher mantle potential temperatures (1331–1345 °C) (Table S5). Similarly, five barometers were used to independently estimate the mantle melting pressure (Albarede, 1992; Haase, 1996; Lee et al., 2009; McKenzie and Bickle, 1988; Putirka, 2008). Since these barometers are dependent on the temperature, the calculated temperatures from the four thermometers and the average temperature were used for comparison. The samples from late Jurassic dolerite and late Cretaceous basanite yield different mantle pressures ranging from 2.0 to 2.9 GPa (Table S5). The late Jurassic samples are calculated to be derived by 2.6–2.9% partial melting of a deeper mantle source at 87–98 km (2.61–2.93 GPa) (Fig. 10b) than late Cretaceous basanites that were derived from approximately 3.5–6.6% partial melting of a mantle source at 67–77 km (2.04–2.33 GPa) (Fig. 10b; Table S5). Given the calculated composition uncertainty of 0.3–0.8% (e.g., Herzberg et al., 2007; Wang et al., 2011),

heterogeneity of mantle composition and different of experient melts and natural samples (e.g., Albarede, 1992; Herzberg and O'hara, 2002), the relative standard deviations of calculated temperature and pressure are 20–46 °C and 0.4–1.4 GPa, respectively (Table S5).

The crystallisation pressures and temperatures of the Bandatso dolerites and basalts were also calculated using the clinopyroxene-liquid thermobarometer (Neave and Putirka, 2017). In order to obtain robust results, the clinopyroxene-melt equilibrium has been assessed for all selected clinopyroxene-liquid pairs using their Fe—Mg exchange coefficient, which was defined as $KD^{cpx\text{-}liq}_{(Fe-Mg)} = [(X^{cpx}_{Fe} \times X^{liq}_{Mg})/(X^{cpx}_{Mg} \times X^{liq}_{Fe})]$ with values within a range of 0.27 ± 0.03 (Fig. 10a; Putirka, 2008), before performing calculations. The calculated P–T results (0.7–1.3 GPa and 1105–1180 °C) suggest an upper crustal magma reservoir and feeding system (at 20–40 km depth) for the Bandatso mafic rocks (Fig. 10b).

### 5.4. Implications

The essential role of heterogeneous multi-terrane configuration in the formation and evolution of large collisional orogens has been increasingly recognised over the last few years (e.g., Huangfu et al., 2018; Kelly et al., 2016; Kelly et al., 2020). The pre-collisional properties of these terranes ultimately determine the evolution of orogen. The Himalaya-Tibet orogen is a heterogeneous multi-terrane collisional orogen (Huangfu et al., 2018; Kelly et al., 2020) with complex tectonomagmatic terranes that were accreted to Asia prior to the collision of India (e.g., Chung et al., 2005). The properties of each major block in the Himalaya-Tibet orogen are critical for our understanding of the lithospheric behaviour and evolution of Tibetan Plateau. However, there was little knowledge of the pre-collisional geology and lithospheric properties of the northern Qiangtang subterrane, which has hitherto only been the focus of a small amount of petrological and geological work due to scarcity of magmatic activity in central Tibet. The current study has helped to redress this imbalance by placing petrological constrains on pre-collisional lithospheric properties and below we propose a two-stage evolution model for the northern Qiangtan during Late Mesozoic.

The calculations reported in the previous section support the presence of a moderately hot (1225–1240 °C) carbonated lithosphere, 90–100 km thick, beneath central Tibet during the Late Jurassic. This is consistent with the late Jurassic (150–120 Ma) flat subduction model of the Bangong-Nujiang Tethyan (Zhang et al., 2017) or the Neo-Tethyan slab (Ma et al., 2013). Generally, during flat subduction, hot asthenosphere at the base of the overriding continental lithosphere is replaced by cold oceanic lithosphere (e.g., Axen et al., 2018), meaning that a large-scale cold thermal structure is expected (e.g., Gutscher, 2018). A new thermo-mechanical model to investigate the dynamic evolution of the Farallon plate beneath the North American continent indicates that the flat subduction can scrape 20–50 km of thick continental lithospheric mantle from the base of the overriding plate (Axen et al., 2018). If the scraped material is relatively light in density, it can accumulate at the front of the subducting plate and form a 'bulldozed keel' (Axen et al., 2018). The asthenospheric wedge is replaced by a mixture of scraped-off lithospheric mantle and oceanic crust, inhibiting melting of the asthenospheric wedge and eventually leading to weakening or termination of arc magmatism and lithospheric thickening. The late Jurassic to early Cretaceous magmatic gaps in the southern Qiangtang (ca. 150–120 Ma, Hao et al., 2019; Peng et al., 2020) and the Lhasa blocks (150–110 Ma, Ma et al., 2013) therefore support potential flat subduction (e.g., Zhang et al., 2017). In addition, during flat subduction, the oceanic sediments accumulated in the front of the subducting plate can provide a source of carbonate metasomatism away from the suture.

The results and modelling presented in this paper for the Bandatso basalts support a depleted mantle-like high temperature (1331–1345 °C) source comparable to depleted MORB mantle (1300–1400 °C; Lee et al., 2009), suggesting adiabatic decompression melting of passively upwelling asthenosphere. In addition, the relatively low estimated mantle potential pressure suggests a relatively thin (70–80 km) continental lithosphere beneath Central Tibet during late Cretaceous (ca. 90 Ma). Based on all above evidence, we propose that a delamination of part of bulldozed keel and high-density oceanic crust caused passively upwelling of asthenosphere to interact with former carbonated lithosphere beneath the northern Qiangtang during roll-back of subducting plate (e.g., Ma et al., 2013, 2015).

Combined with the mantle phlogopite xenocrysts found in Eocene potassic rocks in the eastern Qiangtang (Goussin et al., 2020), our study indicates an inherited pre-collisional carbonated lithospheric mantle beneath the northern Qiangtang that was formed by metasomatism of oceanic sediments during late Jurassic flat subduction. In late Cretaceous, part of the scraped-off lithospheric mantle and high-density oceanic lithosphere at the front of subducting plate were likely delaminated to trigger

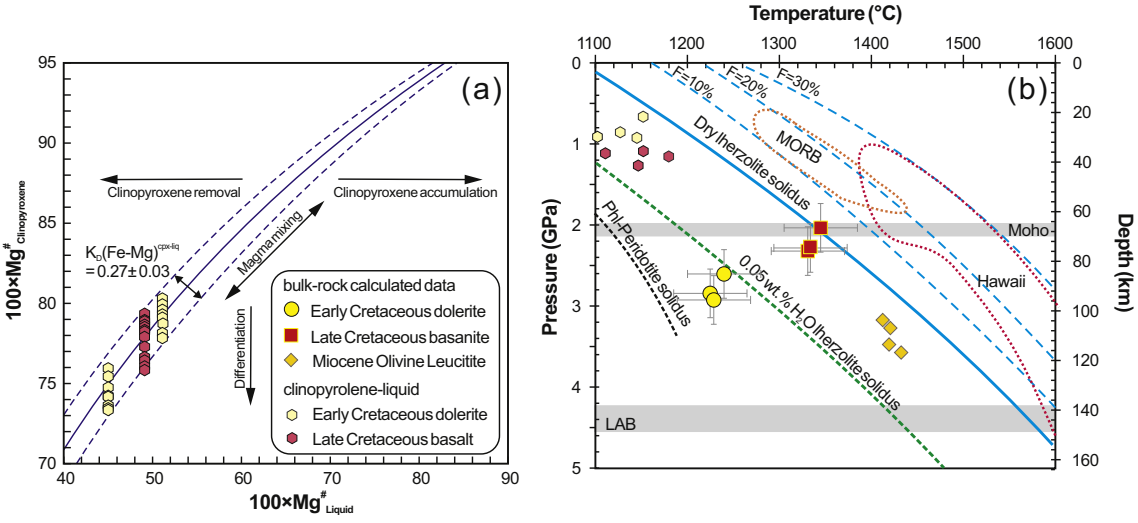


**Fig. 10.** (a) Assessment of clinopyroxene-melt equilibrium. KD values within a range of 0.27 ± 0.03 (Putirka, 2008) were regarded to signify chemical equilibrium.; (b) Temperatures and pressures calculated for Bandatso mafic rocks from Northern Qiangtang. Phl-Peridotite solidus represents the solidus of phlogopite-bearing peridotite containing 0.4 wt% water content and is from Condamine et al. (2016). Solidus lines for dry lherzolite and 0.05 wt% water content lherzolite are from Katz et al. (2003). Depths of the Moho and the lithosphere–asthenosphere boundary (LAB) are from Jiménez-Munt et al. (2008) and Zhang et al. (2011). Miocene olivine leucitite data are from Qi et al. (2020).

decompression melting of the asthenosphere, which further weakened the lithosphere beneath the northern Qiangtang to form the Bandatso mafic rocks in the present study.

A pre-collisional northern continuation of the modern Indian continent is known as Greater India and is postulated to extend approximately 2400 km underneath the Himalayas and southern Tibet (Ingalls et al., 2016). These massive amounts of continental material may help explain the double thickness of Tibetan continental crust (Chung et al., 2009 and references therein). Alternatively, most may have been delaminated or subducted below the over-riding Asian plate (Ingalls et al., 2016; Ma et al., 2017) or may have been accommodated by shortening (e.g., Kapp and DeCelles, 2019; Li et al., 2018). However, given the lack of coeval Lhasa crust shortening and associated deformation of the overlying northern Qiangtang and adjacent Songpan-Ganzi crust (Kapp and DeCelles, 2019), approximately half of the present India-Asia convergence is likely accommodated north of 32°N (Zhang et al., 2004). All these require a weak lithosphere in the northern Qiangtang. Our study is the first to report Late Mesozoic magmatism in the northern Qiangtang and reveals occurrence of a carbonated lithosphere formed by the metasomatism of subducted oceanic sediments during the late Jurassic. This weak inherited lithosphere helps to significantly accommodate the convergence in central Tibet.

Cenozoic magmatic rocks scattered throughout the plateau have been used to decipher the history and mechanisms of plateau uplift (e.g., Chung et al., 2005; Ding et al., 2003; Guo and Wilson, 2019; Turner et al., 1993, 1996; Williams et al., 2004). The Cenozoic potassic rocks with extremely enriched Sr—Nd isotopic compositions are closely associated with the south-to-north rift and have been regarded as the products of uplift (Chung et al., 2005; Ding et al., 2003; Guo et al., 2006; Turner et al., 1993, 1996; Williams et al., 2004). However, as the timing and mechanism for the formation of the enriched mantle sources are unclear, their petrogenesis and origin is still controversial (e.g., Chung et al., 2005; Guo et al., 2015; Ma et al., 2017).

This has also caused a further debate on the mechanism of Tibetan Plateau uplift. There are two competing models to explain the formation of the enriched lithospheric mantle. The “pre-collisional” model suggests that the enrichment was either inherited from the pre-existing ancient lithospheric mantle (Turner et al., 1993, 1996), or was metasomatized by subducted Tethyan oceanic material (Ding et al., 2007). The other model proposes metasomatism by subducted continental material after the India–Asia collision (Guo et al., 2006; Ma et al., 2017). Given the quite different composition between the Cenozoic potassic rocks and late Mesozoic sodic rocks in this study (Figs. 5 and 7), we propose that the enriched mantle source of Cenozoic potassic magmatic rocks was formed after late Cretaceous (ca. 90 Ma). Furthermore, we would argue that continental subduction is very likely to have played a significant role in the thickening and detachment of the Qiangtang lithosphere and uplift of Tibetan Plateau (e.g., Guo et al., 2006; Tapponnier et al., 2001).

## 6. Conclusions

1) The Late Mesozoic Bandatso sodic mafic rocks are characterised by OIB-like compositional features of marked enrichment in incompatible elements.
2) The late Jurassic Bandatso dolerites were formed by melting of carbonated lithosphere metasomatized by subducted oceanic sediments during flat subduction at mantle temperatures of 1225–1240 °C and depths of 90–100 km.
3) The late Cretaceous basanites were likely derived from interaction of lithosphere with asthenosphere upwelling that was induced by removal of previous scraped-off lithosphere and subducted slab.
4) This inherited weak lithosphere beneath northern Qiangtang has likely played a critical role in determining the post-collisional evolution of Himalaya-Tibet orogen.

## Declaration of Competing Interest

The authors declare that they have no known competing financial interests or personal relationships that could have appeared to influence the work reported in this paper.

## Acknowledgments

We thank editor in chief Prof. Michael Roden and Prof. Rene Maury and anonymous reviewer for their valuable suggestions and comments that helped us improve the paper substantially. We appreciate the assistance of Hua-Ning Qiu, Yue–Heng Yang, Xi-Rong Liang, Jin–Long Ma, Xiu-Juan Bai, Ying Liu, Guang–Qian Hu, Xiang–Lin Tu and Le Zhang for zircon age and whole rock geochemical analyses. Financial support for this research was provided by the Second Tibetan Plateau Scientific Expedition and Research (STEP) (2019QZKK0702), the National Natural Science Foundation of China (Nos. 41872062, 91855215 and 41630208), the Strategic Priority Research Program (A) of the Chinese Academy of Sciences (No. XDA2007030402), the National Key Research and Development Project (2016YFC0600309), and the Youth Innovation Promotion Association CAS (2017404). This is contribution No. IS-2986 from GIGCAS.

The data supporting these conclusions can be found in supporting information and EarthChem Library (Ma, L., 2021. Element and Sr—Nd analyses of volcanic rocks from the northern Qiangtang, Tibet, https://doi.org/10.26022/IEDA/111898).

## Appendix A. Supplementary data

Supplementary data to this article can be found online at https://doi.org/10.1016/j.lithos.2021.106076.

## References

Albarede, F., 1992. How deep do common basaltic magmas form and differentiate? J. Geophys. Res. Solid Earth 97, 10997–11009.
Axen, G.J., van Wijk, J.W., Currie, C.A., 2018. Basal continental mantle lithosphere displaced by flat-slab subduction. Nat. Geosci. 11, 961–964.
Bai, X.-J., Qiu, H.-N., Liu, W.-G., Mei, L.-F., 2018. Automatic 40 Ar/39 Ar dating techniques using multicollector ARGUS VI noble gas mass spectrometer with self-made peripheral apparatus. J. Earth Sci. 29, 408–415.
Beattie, P., Ford, C., Russell, D., 1991. Partition coefficients for olivine-melt and orthopyroxene-melt systems. Contrib. Mineral. Petrol. 109, 212–224.
Chauvel, C., McDonough, W., Guille, G., Maury, R., Duncan, R., 1997. Contrasting old and young volcanism in Rurutu Island, Austral chain. Chem. Geol. 139, 125–143.
Chazot, G., Menzies, M.A., Harte, B., 1996. Determination of partition coefficients between apatite, clinopyroxene, amphibole, and melt in natural spinel lherzolites from Yemen: implications for wet melting of the lithospheric mantle. Geochim. Cosmochim. Acta 60, 423–437.
Chen, M., Niu, F., Tromp, J., Lenardic, A., Lee, C.-T.A., Cao, W., Ribeiro, J., 2017. Lithospheric foundering and underthrusting imaged beneath Tibet. Nat. Commun. 8, 15659.
Chung, S.-L., Lo, C.-H., Lee, T.-Y., Zhang, Y., Xie, Y., Li, X., Wang, K.-L., Wang, P.-L., 1998. Diachronous uplift of the Tibetan plateau starting 40 Myr ago. Nature 394, 769–773.
Chung, S.-L., Chu, M.-F., Ji, J. -Q., O'Reilly, S.-Y., Pearson, N., Liu, D.-Y., Lee, T.-Y., Lo, C.-H., 2009. The nature and timing of crustal thickening in Southern Tibet: Geochemical and zircon Hf isotopic constraints from postcollisional adakites. Tectonophysics 477 (1–2), 36–48.
Chung, S.L., Chu, M.F., Zhang, Y., Xie, Y., Lo, C.H., Lee, T.Y., Lan, C.Y., Li, X., Zhang, Q., Wang, Y., 2005. Tibetan tectonic evolution inferred from spatial and temporal variations in post-collisional magmatism. Earth Sci. Rev. 68, 173–196.
Condamine, P., Médard, E., Devidal, J.-L., 2016. Experimental melting of phlogopite-peridotite in the garnet stability field. Contrib. Mineral. Petrol. 171, 95.
Condie, K.C., 2005. High field strength element ratios in Archean basalts: a window to evolving sources of mantle plumes? Lithos 79, 491–504.
Dan, W., Wang, Q., White, W.M., Li, X.-H., Zhang, X.-Z., Tang, G.-J., Ou, Q., Hao, L.-L., Qi, Y., 2020. Passive-Margin Magmatism Caused by Enhanced Slab-Pull Forces in Central Tibet Geology. https://doi.org/10.1130/G47957.47951.
Deng, W., 1998. Cenozoic Intraplate Volcanic Rocks in the Northern Qinghai-Xizang Plateau. Geological Publishing House.
Deng, Y., Tesauro, M., 2016. Lithospheric strength variations in mainland China: Tectonic implications. Tectonics 35, 2313–2333.
Ding, L., Kapp, P., Zhong, D., Deng, W., 2003. Cenozoic volcanism in Tibet: evidence for a transition from oceanic to continental subduction. J. Petrol. 44, 1833–1865.
Ding, L., Kapp, P., Yue, Y., Lai, Q., 2007. Postcollisional calc-alkaline lavas and xenoliths from the southern Qiangtang terrane, Central Tibet. Earth Planet. Sci. Lett. 254, 28–38.

Dupont-Nivet, G., Krijgsman, W., Langereis, C.G., Abels, H.A., Dai, S., Fang, X., 2007. Tibetan plateau aridification linked to global cooling at the Eocene–Oligocene transition. Nature 445, 635–638.
Dupuy, C., Liotard, J., Dostal, J., 1992. Zr/Hf fractionation in intraplate basaltic rocks: carbonate metasomatism in the mantle source. Geochim. Cosmochim. Acta 56, 2417–2423.
England, P., Houseman, G., 1986. Role of lithospheric strength heterogeneities in the tectonics of Tibet and neighbouring regions. Nature 315, 297–301.
Falloon, T.J., Danyushevsky, L.V., 2000. Melting of refractory mantle at 1.5, 2 and 2.5 GPa under anhydrous and $H_2O$-undersaturated conditions: Implications for the petrogenesis of high-Ca boninites and the influence of subduction components on mantle melting. J. Petrol. 41 (2), 257–283.
Goussin, F., Riel, N., Cordier, C., Guillot, S., Boulvais, P., Roperch, P., Replumaz, A., Schulmann, K., Dupont-Nivet, G., Rosas, F., Guo, Z., 2020. Carbonated inheritance in the eastern tibetan lithospheric mantle: petrological evidences and geodynamic implications. Geochem. Geophys. Geosyst. 21, e2019GC008495.
Guo, Z., Wilson, M., 2019. Late Oligocene–early Miocene transformation of postcollisional magmatism in Tibet. Geology 47, 776–780.
Guo, Z., Wilson, M., Liu, J., Mao, Q., 2006. Post-collisional, potassic and ultrapotassic magmatism of the northern Tibetan Plateau: Constraints on characteristics of the mantle source, geodynamic setting and uplift mechanisms. J. Petrol. 47, 1177–1220.
Guo, Z., Wilson, M., Zhang, M., Cheng, Z., Zhang, L., 2015. Post-collisional ultrapotassic mafic magmatism in South Tibet: Products of partial melting of pyroxenite in the mantle wedge induced by roll-back and delamination of the subducted Indian continental lithosphere slab. J. Petrol. 56, 1365–1406.
Gutscher, M.-A., 2018. Scraped by flat-slab subduction. Nat. Geosci. 11, 890–891.
Haase, K.M., 1996. The relationship between the age of the lithosphere and the composition of oceanic magmas: Constraints on partial melting, mantle sources and the thermal structure of the plates. Earth Planet. Sci. Lett. 144, 75–92.
Hao, L.-L., Wang, Q., Zhang, C., Ou, Q., Yang, J.-H., Dan, W., Jiang, Z.-Q., 2019. Oceanic plateau subduction during closure of the Bangong-Nujiang Tethyan Ocean: Insights from central Tibetan volcanic rocks. GSA Bull. 131, 864–880.
Harrison, T.M., Wenji, C., Leloup, P., Ryerson, F., Tapponnier, P., 1992. An early Miocene transition in deformation regime within the Red River fault zone, Yunnan, and its significance for Indo-Asian tectonics. J. Geophys. Res. Solid Earth 97 (1978–2012), 7159–7182.
Hart, S.R., Hauri, E.H., Oschmann, L.A., Whitehead, J.A., 1992. Mantle Plumes and Entrainment: Isotopic evidence. Science 256, 517–520.
Hastie, A.R., Mitchell, S.F., Kerr, A.C., Minifie, M.J., Millar, I.L., 2011. Geochemistry of rare high-Nb basalt lavas: are they derived from a mantle wedge metasomatised by slab melts? Geochim. Cosmochim. Acta 75, 5049–5072.
Hauri, E.H., Shimizu, N., Dieu, J.J., Hart, S.R., 1993. Evidence for hotspot-related carbonatite metasomatism in the oceanic upper mantle. Nature 365, 221–227.
Herzberg, C., Asimow, P.D., 2008. Petrology of some oceanic island basalts: PRIMELT2. XLS software for primary magma calculation. Geochem. Geophys. Geosyst. 9, Q09001 doi: 09010.01029/02008GC002057.
Herzberg, C., O'hara, M., 2002. Plume-associated ultramafic magmas of Phanerozoic age. J. Petrol. 43, 1857–1883.
Herzberg, C., Asimow, P.D., Arndt, N., Niu, Y., Lesher, C., Fitton, J., Cheadle, M., Saunders, A., 2007. Temperatures in ambient mantle and plumes: Constraints from basalts, picrites, and komatiites. Geochem. Geophys. Geosyst. 8, Q02006 doi:02010.01029/02006GC001390.
Hofmann, A., 1997. Mantle geochemistry: the message from oceanic volcanism. Nature 385, 219–229.
Huangfu, P., Li, Z.-H., Gerya, T., Fan, W., Zhang, K.-J., Zhang, H., Shi, Y., 2018. Multi-terrane structure controls the contrasting lithospheric evolution beneath the western and central–eastern Tibetan plateau. Nat. Commun. 9, 3780.
Ingalls, M., Rowley, D.B., Currie, B., Colman, A.S., 2016. Large-scale subduction of continental crust implied by India–Asia mass-balance calculation. Nat. Geosci. 9, 848–853.
Jackson, M.G., Dasgupta, R., 2008. Compositions of HIMU, EM1, and EM2 from global trends between radiogenic isotopes and major elements in ocean island basalts. Earth Planet. Sci. Lett. 276, 175–186.
Jiménez-Munt, I., Fernàndez, M., Vergés, J., Platt, J.P., 2008. Lithosphere structure underneath the Tibetan Plateau inferred from elevation, gravity and geoid anomalies. Earth Planet. Sci. Lett. 267, 276–289.
Kapp, P., DeCelles, P.G., 2019. Mesozoic–Cenozoic geological evolution of the Himalayan-Tibetan orogen and working tectonic hypotheses. Am. J. Sci. 319, 159–254.
Katz, R.F., Spiegelman, M., Langmuir, C.H., 2003. A new parameterization of hydrous mantle melting. Geochem. Geophys. Geosyst. 4.
Kelly, S., Butler, J.P., Beaumont, C., 2016. Continental collision with a sandwiched accreted terrane: Insights into Himalayan–Tibetan lithospheric mantle tectonics? Earth Planet. Sci. Lett. 455, 176–195.
Kelly, S., Beaumont, C., Butler, J.P., 2020. Inherited terrane properties explain enigmatic post-collisional Himalayan-Tibetan evolution. Geology 48, 8–14.
Koppers, A.A., 2002. ArArCALC—software for 40Ar/39Ar age calculations. Comput. Geosci. 28, 605–619.
Le Bas, M.J., Le Maitre, R., Streckeisen, A., Zanettin, B., 1986. A chemical classification of volcanic rocks based on the total alkali-silica diagram. J. Petrol. 27, 745–750.
Lee, C.-T.A., Luffi, P., Plank, T., Dalton, H., Leeman, W.P., 2009. Constraints on the depths and temperatures of basaltic magma generation on Earth and other terrestrial planets using new thermobarometers for mafic magmas. Earth Planet. Sci. Lett. 279, 20–33.
Li, L., Garzione, C.N., Pullen, A., Zhang, P., Li, Y., 2018. Late Cretaceous–Cenozoic basin evolution and topographic growth of the Hoh Xil Basin, central Tibetan Plateau. GSA Bull. 130, 499–521.
Liu, T., Zhai, Q.-G., Wang, J., Bao, P.-S., Qiangba, Z., Tang, S.-H., Tang, Y., 2016. Tectonic significance of the Dongqiao ophiolite in the north-central Tibetan plateau: evidence from zircon dating, petrological, geochemical and Sr–Nd–Hf isotopic characterization. J. Asian Earth Sci. 116, 139–154.
Ma, L., Wang, Q., Wyman, D.A., Li, Z.-X., Jiang, Z.-Q., Yang, J.-H., Gou, G.-N., Guo, H.-F., 2013. Late cretaceous (100–89Ma) magnesian charnockites with adakitic affinities in the Milin area, eastern Gangdese: partial melting of subducted oceanic crust and implications for crustal growth in southern Tibet. Lithos 175, 315–332.
Ma, L., Wang, Q., Wyman, D.A., Jiang, Z.Q., Wu, F.Y., Li, X.H., Yang, J.H., Gou, G.N., Guo, H.F., 2015. Late cretaceous back-arc extension and arc system evolution in the Gangdese area, southern Tibet: Geochronological, petrological, and Sr-Nd-Hf-O isotopic evidence from Dagze diabases. J. Geophys. Res. Solid Earth 120, 6159–6181.
Ma, L., Wang, Q., Li, Z.-X., Wyman, D.A., Yang, J.-H., Jiang, Z.-Q., Liu, Y.-S., Gou, G.-N., Guo, H.-F., 2017. Subduction of Indian continent beneath southern Tibet in the latest Eocene (~35Ma): Insights from the Quguosha gabbros in southern Lhasa block. Gondwana Res. 41, 77–92.
Ma, L., Kerr, A.C., Wang, Q., Jiang, Z.Q., Tang, G.J., Yang, J.H., Xia, X.P., Hu, W.L., Yang, Z.Y., Sun, P., 2019. Nature and Evolution of Crust in Southern Lhasa, Tibet: Transformation from Microcontinent to Juvenile Terrane. J. Geophys. Res. Solid Earth 124, 6452–6474.
McKenzie, D., Bickle, M., 1988. The volume and composition of melt generated by extension of the lithosphere. J. Petrol. 29, 625–679.
McKenzie, D., O'Nions, R.K., 1995. The Source Regions of Ocean Island Basalts. J. Petrol. 36, 133–159.
Murphy, M., Yin, A., Harrison, T.M., Dürr, S.B., Chen, Z.D., Ryerson, F.J., Kidd, W.S.F., Wang, X., Zhou, X., 1997. Did the Indo-Asian collision alone create the Tibetan Plateau? Geology 25, 719–722.
Neave, D.A., Putirka, K.D., 2017. A new clinopyroxene-liquid barometer, and implications for magma storage pressures under Icelandic rift zones. Am. Mineral. 102, 777–794.
Niu, Y.-L., 2008. The origin of alkaline lavas. Science 320 (5878), 883–884.
Ou, Q., Wang, Q., Wyman, D.A., Zhang, H.X., Yang, J.H., Zeng, J.P., Hao, L.L., Chen, Y.W., Liang, H., Qi, Y., 2017. Eocene adakitic porphyries in the central-northern Qiangtang Block, Central Tibet: Partial melting of thickened lower crust and implications for initial surface uplifting of the plateau. J. Geophys. Res. Solid Earth 122, 1025–1053.
Ou, Q., Wang, Q., Wyman, D.A., Zhang, C., Hao, L.-L., Dan, W., Jiang, Z.-Q., Wu, F.-Y., Yang, J.-H., Zhang, H.-X., 2019. Postcollisional delamination and partial melting of enriched lithospheric mantle: evidence from Oligocene (ca. 30 Ma) potassium-rich lavas in the Gemuchaka area of the central Qiangtang Block, Tibet. Geol. Soc. Am. Bull. 131, 1385–1408.
Pearce, J.A., Peate, D.W., 1995. Tectonic implications of the composition of volcanic arc magmas. Annu. Rev. Earth Planet. Sci. 23, 251–286.
Peng, Y., Yu, S., Li, S., Liu, Y., Santosh, M., Lv, P., Li, Y., Xie, W., Liu, Y., 2020. The odyssey of Tibetan Plateau accretion prior to Cenozoic India-Asia collision: probing the Mesozoic tectonic evolution of the Bangong-Nujiang Suture. Earth Sci. Rev. 211, 103376.
Pfänder, J.A., Jung, S., Münker, C., Stracke, A., Mezger, K., 2012. A possible high Nb/Ta reservoir in the continental lithospheric mantle and consequences on the global Nb budget – evidence from continental basalts from Central Germany. Geochim. Cosmochim. Acta 77, 232–251.
Pilet, S., Baker, M.B., Stolper, E.M., 2008. Metasomatized lithosphere and the origin of alkaline lavas. Science 320, 916–919.
Putirka, K.D., 2005. Mantle potential temperatures at Hawaii, Iceland, and the mid-ocean ridge system, as inferred from olivine phenocrysts: Evidence for thermally driven mantle plumes. Geochem. Geophys. Geosyst. 6. https://doi.org/10.1029/2005GC000915.
Putirka, K.D., 2008. Thermometers and barometers for volcanic systems. Rev. Mineral. Geochem. 69, 61–120.
Qi, Y., Wang, Q., Zhu, Y.-T., Shi, L.-C., Yang, Y.-N., 2020. Miocene olivine leucitites in the Hoh Xil Basin, Northern Tibet: implications for intracontinental lithosphere melting and surface uplift of the Tibetan Plateau. J. Petrol. 61.
Royden, L.H., Burchfiel, B.C., van der Hilst, R.D., 2008. The geological evolution of the Tibetan Plateau. Science 321, 1054–1058.
Rudnick, R., Gao, S., 2003. Composition of the continental crust. Treatise Geochem. 3, 1–64.
Shi, D., Klemperer, S.L., Shi, J., Wu, Z., Zhao, W., 2020. Localized foundering of Indian lower crust in the India–Tibet collision zone. Proc. Natl. Acad. Sci. 117, 24742–24747.
Sobolev, A.V., Hofmann, A.W., Sobolev, S.V., Nikogosian, I.K., 2005. An olivine-free mantle source of Hawaiian shield basalts. Nature 434, 590–597.
Sugawara, T., 2000. Empirical relationships between temperature, pressure, and MgO content in olivine and pyroxene saturated liquid. J. Geophys. Res. Solid Earth 105, 8457–8472.
Sun, S.S., McDonough, W., 1989. Chemical and isotopic systematics of oceanic basalts: implications for mantle composition and processes. Geol. Soc. Lond., Spec. Publ. 42, 313–345.
Tamura, Y., Yuhara, M., Ishii, T., 2000. Primary Arc Basalts from Daisen Volcano, Japan: Equilibrium Crystal Fractionation versus Disequilibrium Fractionation during Supercooling. J. Petrol. 41, 431–448.
Tang, Y., Zhai, Q.-G., Chung, S.-L., Hu, P.-Y., Wang, J., Xiao, X.-C., Song, B., Wang, H.-T., Lee, H.-Y., 2020. First mid-ocean ridge-type ophiolite from the Meso-Tethys suture zone in the north-central Tibetan plateau. GSA Bull. 132, 2202–2220.
Tapponnier, P., Zhiqin, X., Roger, F., Meyer, B., Arnaud, N., Wittlinger, G., Jingsui, Y., 2001. Oblique stepwise rise and growth of the Tibet Plateau. Science 294, 1671–1677.
Tatsumi, Y., Eggins, S.M., 1995. Subduction Zone Magmatism. Blackwell, Cambridge.
Turner, S., Hawkesworth, C., Liu, J.Q., Rogers, N., Kelley, S., Van Calsteren, P., 1993. Timing of Tibetan uplift constrained by analysis of volcanic rocks. Nature 364, 50–54.
Turner, S., Arnaud, N., LIU, J., Rogers, N., Hawkesworth, C., Harris, N., Kelley, S.v., Van Calsteren, P., Deng, W., 1996. Post-collision, shoshonitic volcanism on the Tibetan Plateau: implications for convective thinning of the lithosphere and the source of ocean island basalts. J. Petrol. 37, 45–71.

Wang, Q., Wyman, D.A., Xu, J., Dong, Y., Vasconcelos, P.M., Pearson, N., Wan, Y., Dong, H., Li, C., Yu, Y., Zhu, T., Feng, X., Zhang, Q., Zi, F., Chu, Z., 2008. Eocene melting of subducting continental crust and early uplifting of Central Tibet: evidence from central-western Qiangtang high-K calc-alkaline andesites, dacites and rhyolites. Earth Planet. Sci. Lett. 272, 158–171.

Wang, Q., Wyman, D.A., Li, Z.-X., Sun, W., Chung, S.-L., Vasconcelos, P.M., Zhang, Q., Dong, H., Yu, Y., Pearson, N., 2010. Eocene north–south trending dikes in Central Tibet: new constraints on the timing of east–west extension with implications for early plateau uplift? Earth Planet. Sci. Lett. 298, 205–216.

Wang, X.-C., Li, Z.-X., Li, X.-H., Li, J., Liu, Y., Long, W.-G., Zhou, J.-B., Wang, F., 2011. Temperature, pressure, and composition of the mantle source region of late Cenozoic basalts in Hainan Island, SE Asia: a consequence of a young thermal mantle plume close to subduction zones? J. Petrol. 53, 177–233.

Wang, X.-C., Wilde, S.A., Li, Q.-L., Yang, Y.-N., 2015. Continental flood basalts derived from the hydrous mantle transition zone. Nat. Commun. 6, 7700.

Williams, H., Turner, S., Pearce, J., Kelley, S., Harris, N., 2004. Nature of the source regions for post-collisional, potassic magmatism in southern and northern Tibet from geochemical variations and inverse trace element modelling. J. Petrol. 45, 555–607 https://doi.org/510.1093/petrology/egg1094.

Woodhead, J.D., 1996. Extreme HIMU in an oceanic setting: the geochemistry of Mangaia Island (Polynesia), and temporal evolution of the Cook—Austral hotspot. J. Volcanol. Geotherm. Res. 72, 1–19.

Xu, W., Liu, F., Dong, Y., 2020. Cambrian to Triassic geodynamic evolution of central Qiangtang, Tibet. Earth Sci. Rev. 201, 103083.

Yang, J., Faccenda, M., 2020. Intraplate volcanism originating from upwelling hydrous mantle transition zone. Nature 579, 88–91.

Yin, A., Harrison, T.M., 2000. Geologic evolution of the Himalayan-Tibetan orogen. Annu. Rev. Earth Planet. Sci. 28, 211–280.

Zhang, P.-Z., Shen, Z., Wang, M., Gan, W., Bürgmann, R., Molnar, P., Wang, Q., Niu, Z., Sun, J., Wu, J., Hanrong, S., Xinzhao, Y., 2004. Continuous deformation of the Tibetan Plateau from global positioning system data. Geology 32, 809–812.

Zhang, X.-Z., Wang, Q., Dong, Y.-S., Zhang, C.-F., Li, Q.-Y., Xia, X.-P., Xu, W., 2017. High-Pressure Granulite Facies Overprinting During the Exhumation of Eclogites in the Bangong- Nujiang Suture Zone, Central Tibet: Link to Flat-Slab Subduction. Tectonics 36. https://doi.org/10.1002/2017TC004774.

Zhang, Q., Sandvol, E., Ni, J., Yang, Y., Chen, Y.J., 2011. Rayleigh wave tomography of the northeastern margin of the Tibetan Plateau. Earth Planet. Sci. Lett. 304, 103–112.

Zhang, X.Z., Dong, Y.S., Wang, Q., Dan, W., Zhang, C., Deng, M.R., Xu, W., Xia, X.P., Zeng, J.P., Liang, H., 2016. Carboniferous and Permian evolutionary records for the Paleo-Tethys Ocean constrained by newly discovered Xiangtaohu ophiolites from central Qiangtang, Central Tibet. Tectonics 35, 1670–1686.

Zhu, D.-C., Zhao, Z.-D., Niu, Y., Dilek, Y., Hou, Z.-Q., Mo, X.-X., 2013. The origin and pre-Cenozoic evolution of the Tibetan Plateau. Gondwana Res. 23, 1429–1454.